Smart Structures and Systems, *Vol. 24, No. 5 (2019) 641-648*
DOI: https://doi.org/10.12989/sss.2019.24.5.641

Vision-based support in the characterization of superelastic U-shaped SMA elements

F. Casciati[1a], S. Casciati[*2], A. Colnaghi[2b], L. Faravelli[1c], L. Rosadini[2d] and S. Zhu[3e]

[1]Dicar, University of Pavia, via Ferrata 3, 27100 Pavia, Italy
[2]SIART srl, via dei Mille 73, 27100 Pavia, Italy
[3]Department of Civil and Environmental Engineering, The Hong Kong Polytechnic University, Hong Kong, China

(Received June 12, 2019, Revised August 14, 2019, Accepted August 23, 2019)

Abstract. The authors investigate the feasibility of applying a vision-based displacement-measurement technique in the characterization of a SMA damper recently introduced in the literature. The experimental campaign tests a steel frame on a uni-axial shaking table driven by sinusoidal signals in the frequency range from 1Hz to 5Hz. Three different cameras are used to collect the images, namely an industrial camera and two commercial smartphones. The achieved results are compared. The camera showing the better performance is then used to test the same frame after its base isolation. U-shaped, shape-memory-alloy (SMA) elements are installed as dampers at the isolation level. The accelerations of the shaking table and those of the frame basement are measured by accelerometers. A system of markers is glued on these system components, as well as along the U-shaped elements serving as dampers. The different phases of the test are discussed, in the attempt to obtain as much possible information on the behavior of the SMA elements. Several tests were carried out until the thinner U-shaped element went to failure.

Keywords: base isolation; camera; shaking table test; shape memory alloy; vision-based technology

1. Introduction

At the International Conference on Digital Image Correlation and Noncontact Experimental Mechanics (IDICS2018), held in Hangzhou on October 2018, this research group outlined as two main aspects are critical in view of successful applications of vision-based technology in structural monitoring and experimental mechanics: the camera features and the open accessibility to the elaboration software.

The second aspect is covered by the migration from proprietary software for image processing to codes easily obtained by assembling routines in software environments as MatLab®.

The first aspect shows two conflictual points of view: the cost of the camera device versus the need of higher technological properties, such as a higher frame-per-second capacity, a higher precision in recording the time of the shot, and an improved quality of the image storage.

This paper first discusses in detail the camera selection and, then, moves to an application to catch the response of shape memory alloy (SMA) components. Therefore, the next section is devoted to compare the accuracy obtained and the effort required when using three different types of camera devices. In particular, the potential of smartphones (Zhao *et al*. 2019, Sony *et al*. 2019) is discussed, even if, to allow their use, the applications have to be limited to mechanical problems where the frequency content of the signals is under 5 Hz (Wu *et al*. 2014).

The remaining part of the paper is devoted to a laboratory experiment exploiting a smartphone as camera and studying the response of U elements in shape memory alloy. The concept was first introduced in a pioneering proposal (Casciati *et al.* 1998). Then, the U-shaped elements were recently developed and implemented in (Wang and Zhu 2018) thanks to a new alloy-processing technology.

2. Vision-based technology and camera features

"Digital Image Correlation" (DIC) (Pan *et al*. 2009, Ye *et al*. 2016a, Pan *et al*. 2018) is the theory on the back of object tracking in vision-based technology. When applied to structural monitoring, it is successful in detecting displacements in a non-contact manner (Ye *et al*. 2013, Wu and Casciati 2014, Ye *et al*. 2016b).

The strength of the approach is its ability to provide a dense (in the plane or in the space) collection of measurements. The location and placement of acquisition cameras allow one to observe an object under different perspectives, which results in the main schemes summarized in Fig. 1.

*Corresponding author, Ph.D.
E-mail: saracasciati@msn.com
[a] Professor
[b] Researcher
[c] Professor
[d] Researcher
[e] Associate Professor

ISSN: 1738-1584 (Print), 1738-1991 (Online)

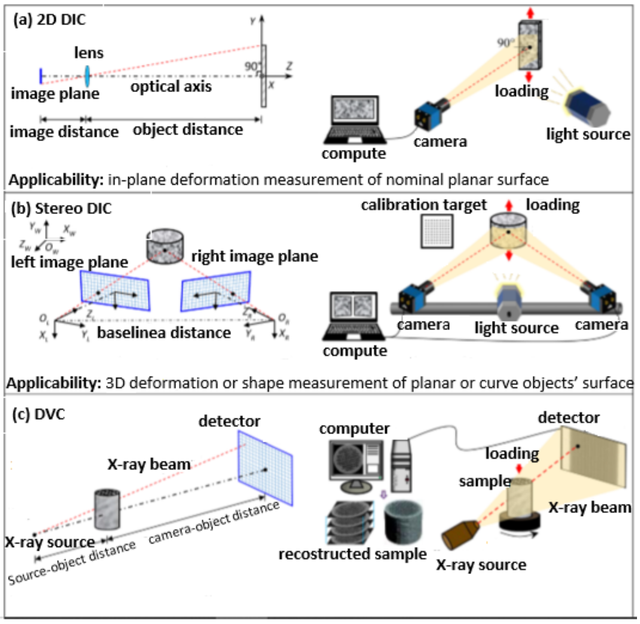

Fig. 1 The main DIC classes: 2D, 3D and DVC (digital volume correlation).

Within a 2D-DIC framework, the images are acquired by a SunTime FX30 camera (Fig. 2), specifically proposed for high-speed acquisition of dynamic images. These images are then compared with the ones obtained by an iPhone 6 (Fig. 2(b)) and a Huawei p20 (Fig. 2(c)).

The devices have different features in terms of acquisition frequency. The camera is sold for 60 fps (frame per second), but in the authors' experience a maximum of 30 fps was achieved and, as underlined below, the acquisition time is not constant. A constant acquisition time belongs to the smartphones, but for the two devices used in this research, the acquisition rate is only 10 fps and 20 fps, respectively. In the remaining of this section, the authors want to emphasize advantages and drawbacks in the attempt to replace cameras by smartphones.

This is done with reference to a case study, which covers a multi-story steel frame mounted on a shaking table with a single degree of freedom (Fig. 3). The steel frame consists of four columns and three steel plates, plus a plate at the bottom. The material properties of the steel members are summarized as follows: the modulus of elasticity is 210,000 MPa, the Poisson ratio 0.3, and the weight per unit of volume 78.500 N / m^3. Tri-axial accelerometers are installed on each floor to identify and monitor the structural system. The first frequency of the frame is 1.26 Hz. The command of the shaking table drives the table following sinusoidal displacements of given span and frequency.

When one adopts a computer vision-based displacement measurement scheme, one needs hardware and software components. The hardware part consists of a commercial camera, a computer for data acquisition and processing, and a set of user-defined target markers. The camera records the marker's movements. They are simultaneously transferred to the computer. The software running in the computer calculates the displacements using image-processing algorithms and coordinate transformations.

(a)

(b)

(c)

Fig. 2 The three devices used as visual-based monitoring systems: (a) the camera SunTime FX30, (b) iPhone 6 and (c) Huawei

The camera used for the acquisition of images is the SunTime FX30 camera already tested in (Wu *et al*. 2014). The main features of this device are summarized as follows. It has a Charge - Coupled Device (CCD) sensor, an 8bit/12bit A/D conversion, the number of effective pixels is 680H by 480V, and the image acquisition speed reaches, as said, up to 30 frames per second. Despite the main features of the smartphone cameras are easily found in the web, they are summarized below. For the iPhone 6: an 8 Mp front camera and an image size of 3264x2448 pixels; for Huawei p20: a 12 Mp front camera and an image size of 4290x2800 pixels.

The markers chosen to perform the experiment in the laboratory are luminous LEDs glued onto the structure. As regards the columns of the model, a very dense configuration is chosen; namely, eight LEDs are placed along each element at a distance of about 4 cm from each other. The choice of such a dense distribution come from the remark that applying a greater number of markers allows one to identify the most accurate deformed configuration.

Only three LEDs cover the horizontal plates whose thickness makes any remarkable bending unlike. Within such a detection scheme, it is always required to place a pair of LEDs on an object at rest as reference. These markers allow one to estimate the displacements relative to their fixed position.

The distance between the camera and the frame is 3m. The software elaborates the displacements in pixel units. In order to determine the conversion factor, the distance between the reference markers is used. As a result, one obtains the value of 2.595 [mm / pixel] for the camera in Figure 2a. Such a camera is in use when exciting the shaking table at the model resonance frequency (1.26 Hz) with a span of 2 mm. The image processing software randomly assigns labels to the markers glued on the structures and those serving as reference (Fig. 4).

In Fig. 4, the reference markers are T12 and T29. They remain coplanar with the structure from the camera point of view. The markers T57 and T58 denote the base of the vibrating table; they are motion control elements since the displacement obtained from their processing must be congruent with the one imposed during the test. The markers characterizing the three floors are T41-43 for the first floor, T21-T23 for the second floor, and T1-3 for the third (and top) floor.

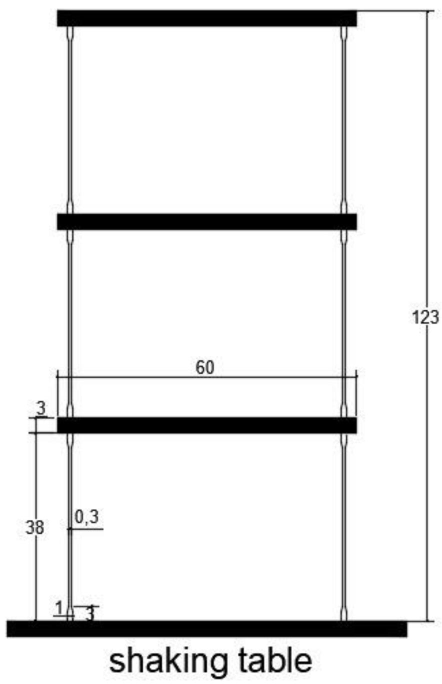

Fig. 3 The steel frame tested as case study. Lengths in centimeters

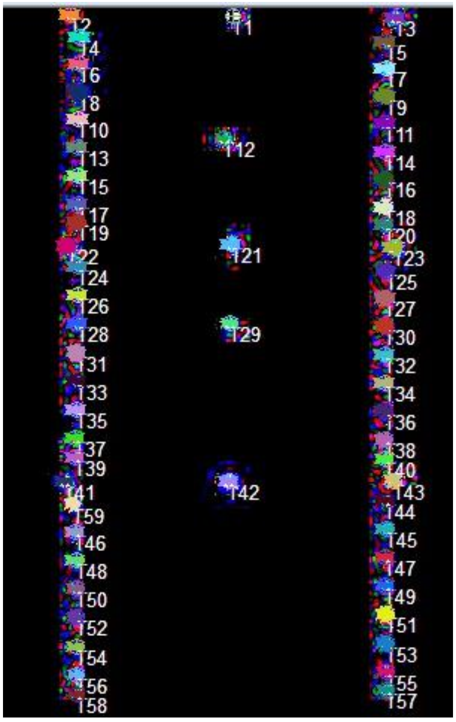

Fig. 4 Labelled markers as resulting from the processing software

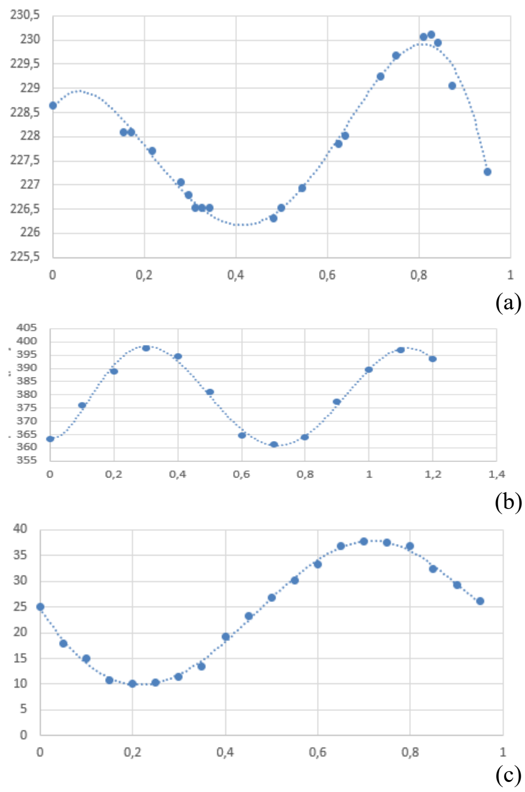

Fig. 5 Segments of the displacement time histories of the top markers as collected by the three devices in Fig. 2: (a) the camera SunTime FX30, (b) iPhone 6 and (c) Huawei. Time along the abscissa in seconds. Ordinates in pixels

Fig. 5 provides a plot of duration 1 sec of the recorded displacement time history for one of the markers on the top of the frame. Actually, a discretized time history is collected. Paying attention to the point abscissae one sees that the subsequent time instants are not equally spaced.

A similar test is carried out by using the other two devices in Fig. 2. The only difference in the process of providing the excitation to the frame consists of imposing a displacement to the top element at the starting time. There is not a specific motivation for this, except that the pursued comparison will be based on a single cycle, thus making a stationary excitation useless.

Recorded time histories for the same marker are also depicted in Fig. 5. The data from the iPhone6 device are equally spaced. The Huawei camera gives a larger number of still equally spaced data points but the accuracy on the curve is lower. This led the authors to prefer the iPhone6 for the developments reported in the next section. Nevertheless, it is worth recalling that with 10 images per second, the investigable frequency just spans from 0 to 5 Hz.

Furthermore, the adoption of a smartphone has its own drawbacks. Namely, the shot comes in a colored large format that must be reduced to a nearly gray-scale small size image to make it editable by the image processing software. Moreover, after 150 shots the storage capacity is full.

3. Testing the U shaped SMA elements

3.1 Experimental mock-up

The stiffness of the frame tested in the previous section is increased by adding braces between all consecutive floors (Fig. 6). Adding the braces makes the superstructure behave like a single degree of freedom system. For this reason, there are no markers on the frame structure in this test.

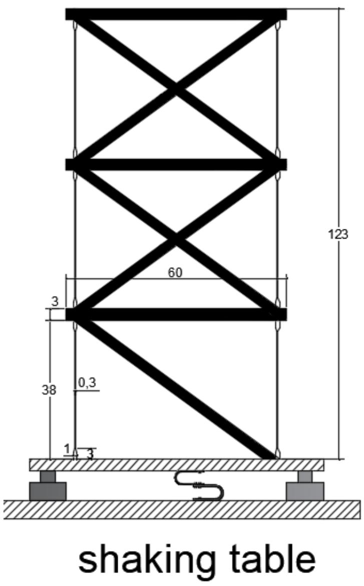

Fig. 6 Adding braces, base isolation (sliding supports) and the U-shaped SMA dampers to the steel frame

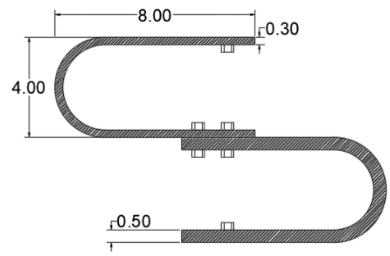

Fig. 7 Details of the damper assemblage. Lengths in cm

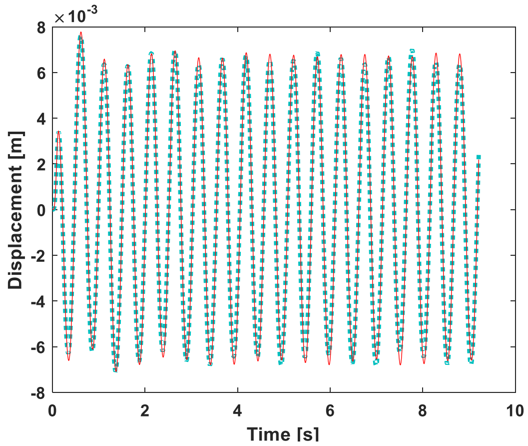

Fig. 8 Comparing the shaking-table displacement time history (solid line) with that of the basement (dotted line) for 2 Hz as frequency of the driving signal. Span 7.2 mm

The basement, originally fixed to the shaking table by bolts, is now standing on two sliding supports and a damper is introduced between the basement and the shaking table. The test results rely on the signals recorded by accelerometers at strategic points: shaking-table, basement and top of the frame structure. The last one is considered jus for checking any possible rotation about the transversal and the vertical axes.

The above mentioned damper is obtained as shown in Fig. 7. The U-shaped superelastic SMA elements come from the producer in two sets of two identical specimens. They show a height of 4 cm and a length of 8 cm, but they differ one from the other for the thickness, of 3 mm and 5 mm, respectively. Wang and Zhu (2018) described the material and the technological process to obtain the U-shape in detail. By holes of diameter 3 mm, the two elements of different thickness are assembled together as in Fig. 7, resulting in an S-shaped damper. They are mounted between the frame base bottom and the shaking tabletop.

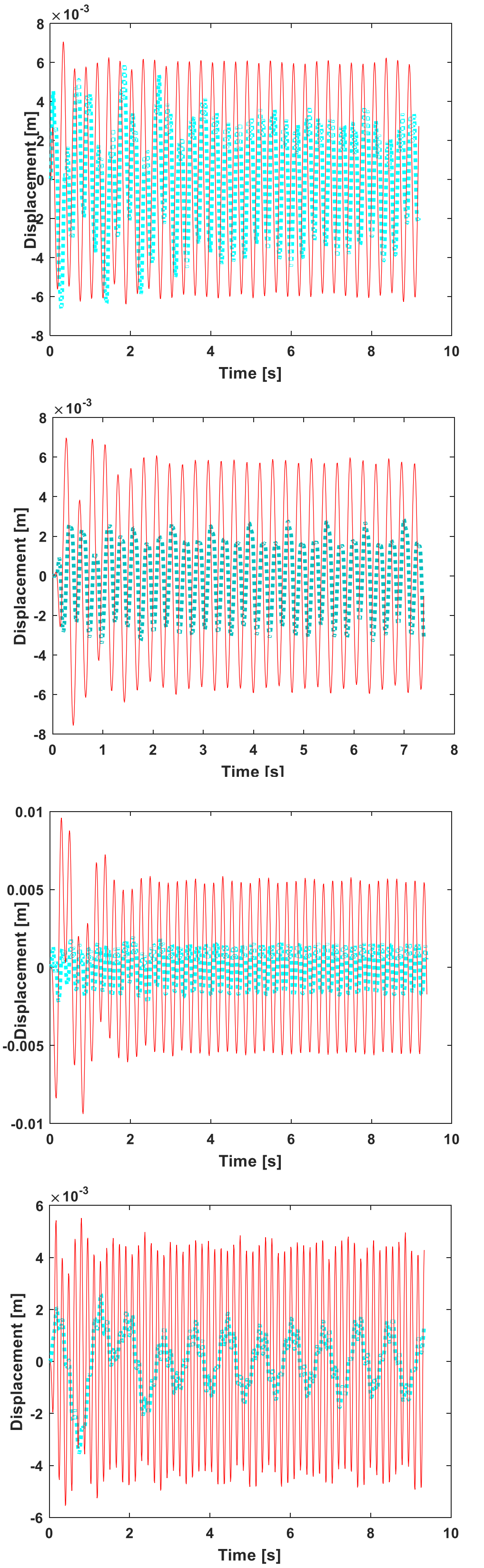

(a)

(b)

(c)

(d)

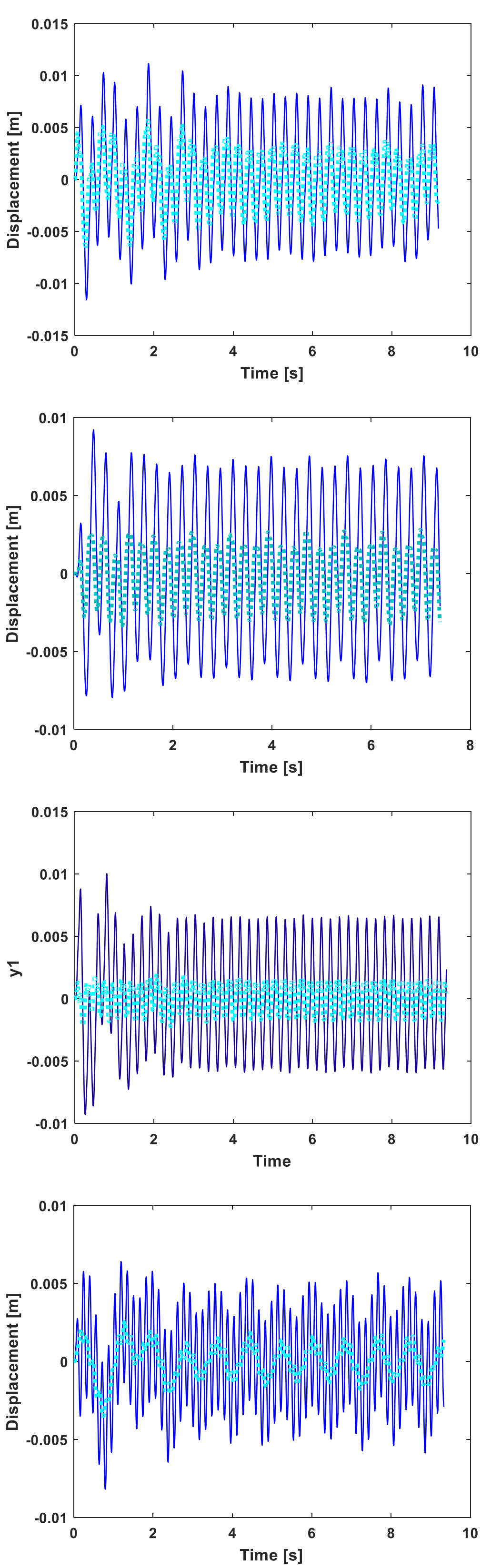

(a)

(b)

(c)

(d)

Fig. 9 Comparing the shaking-table displacement time history (solid line) with that of the basement (dotted line) for different frequencies of the driving signal: (a) 3.44 Hz, (b) 3.89 Hz, (c) 4.4 Hz and (d) 6.3 Hz Span 7.2 mm

Fig. 10 Relative displacement (base minus tabletop; solid line) vs. the frame base displacement time history (dotted line) for the driving frequencies: (a) 3.44 Hz, (b) 3.89 Hz, (c) 4.4 Hz and (d) 6.3 Hz. Span 7.2 mm

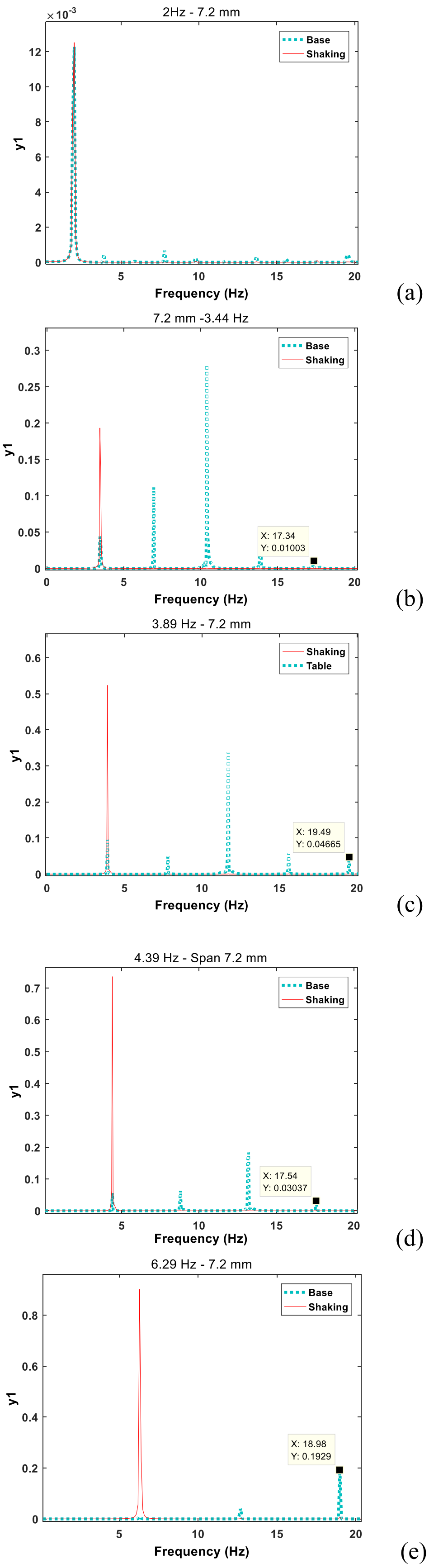

Fig. 11 Comparing the shaking-table acceleration spectrum (solid line) with that of the frame base (dotted line). Frequencies of the driving signal. (a) 2 Hz, (b) 3.44 Hz, (c) 3.89 Hz, (d) 4.4 Hz and (e) 6.3 Hz. Span 7.2 mm

3.2 Accelerometric results

The first step consists of identifying the built mechanical model by the recorded accelerometric signals when exciting the shaking table with different (in frequency) sinusoidal displacement functions. Several tests are repeated by progressively increasing the table span (i.e., the intensity of the sine function) to be sure that the input is tolerable by the system.

A final span of 7.2 mm is deeply investigated and some results are reported in the following.

At the driving frequency of 2 Hz (Fig. 8), the table and the frame-basement move as a single body: no sliding at all. By increasing the driving frequency, the sliding starts and the frequencies associated with the U-shaped SMA elements alter the motion (Fig. 9) and relative motion, between the frame base and the shaking tabletop, can be outlined (Fig. 10). Nevertheless, it is worth noticing that in this frequency range the motion occurs in phase opposition resulting in significant relative displacements that directly affect the SMA behavior. For a driving frequency higher than 7.5 Hz, the classical base-isolation response occurs, with the frame at rest (Casciati *et al.* 2007).

Looking the response from the frequency point of view, the spectra of the accelerations in Fig. 11 emphasizes the gradual reduction of the role of the first harmonic, making the third harmonic as the dominant one.

3.3 Vision-based tests

The adoption of the above discussed vision-based technique requires to apply markers and to track the motion of several points by a sequence of images. The target of the experiment is to collect information on the response of the different points of the SMA elements. Therefore, the markers are placed as in Fig. 12, where a picture of the specimen is also shown.

The LEDs T1 and T2 belong to the frame base, the LEDs labelled from T3 to T9 are glued on the damper profile and the LEDs T12 and T13 belong to the shaking table. Quite important, there are two further LEDs, T10 and T11, on an object isolated from the shaking table: they represent the reference markers.

As introduced at the end of section 2, the camera used is just an iPhone6, with a rate of 10 frames per second. Usually 18 or 24 successive shots are recorded. The distance of the frame from the camera is 50 cm.

With the markers on, three different tests are carried out, all of them with a shaking table span of 7.2 mm. The driving frequency is 2.5 Hz, 4 Hz and 6.25 Hz, respectively. The selection of these values is a direct consequence of the systems response illustrated in Figure 10, where the relative displacements between the frame-base and the shaking table is shown.

The obtained three sequences of iPhone6 shots are first manipulated to make the image editable by the image processing software. This software first creates an image sequence and then applies a multi-tracking algorithm. As a result, the markers coordinates at each subsequent time are obtained and, from here, the displacement estimated.

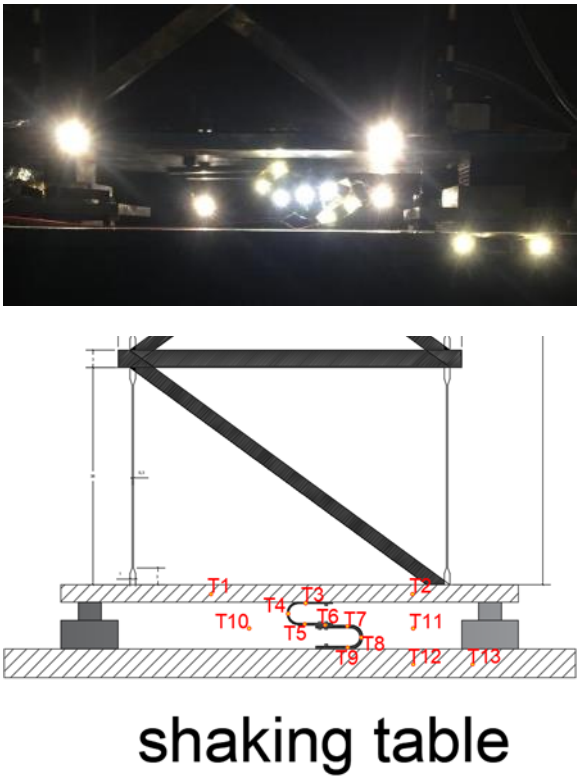

Fig. 12 One of the collected images (top) and labeling of the markers (bottom)

Fig. 13 Detail of the rupture of the thin U-shaped element

The displacements along the motion of some markers are summarized in Figure 14. The sudden failure of one of the two SMA elements of lower thickness prevents the authors from conducting further experiments. But this rupture also leads the authors to recall the fatigue weakness of shape memory alloy as emphasized on bars (Casciati *et al.* 2011), wires (Casciati *et al.* 2017, 2018) as well as on shell elements (Casciati and Faravelli 2008)

5. Conclusions

Vision-based technology requires the availability of a camera. Three different devices are first evaluated, achieving the conclusion that even smartphone cameras can be conveniently used for studying a motion with frequency content up to 5 Hz. Indeed, the use in structural dynamics of cameras requires they mount a device able to record quite accurately the time of the shot. This feature was outlined to be a major must in applications of vision-based technology in structural monitoring.

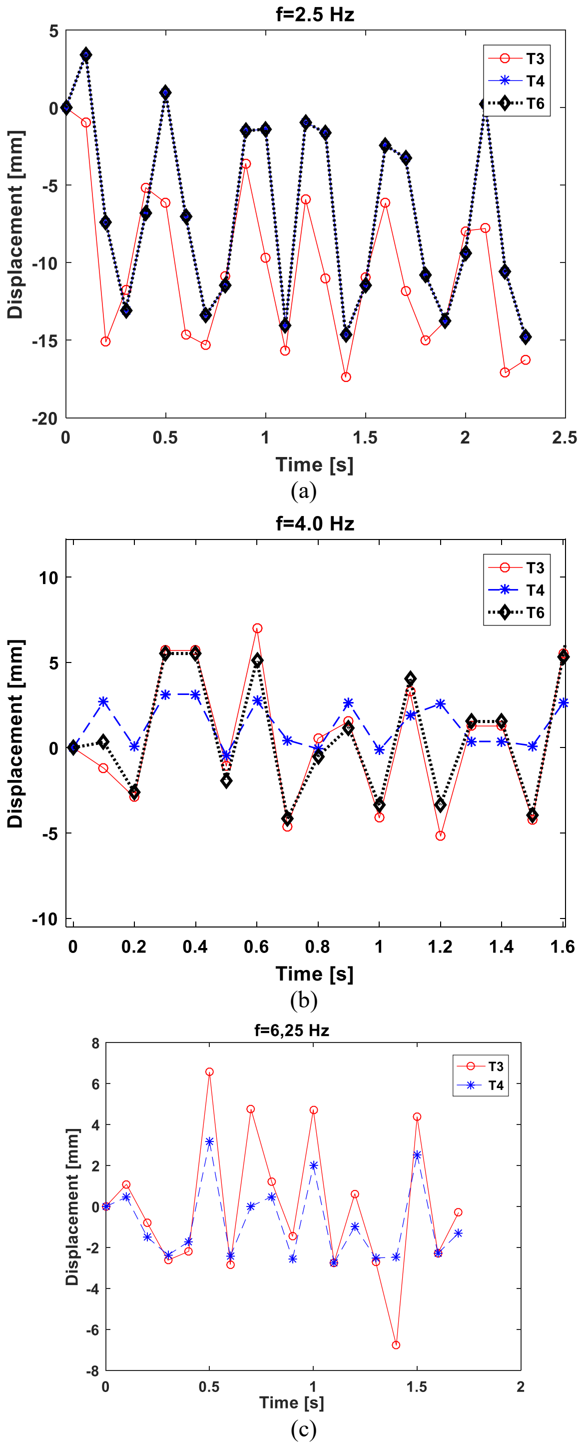

Fig. 14 Recorded displacement time histories of some of the markers on the U-shaped elements. Driving frequency: (a) 2.5 Hz, (b) 4 Hz and 6.25 Hz. Span 7.2 mm

A smartphone is then used to record the motion, driven by a shaking table of a steel frame isolated at the base and mounting U-shaped shape-memory-alloy elements. These elements are obtained by a special cutting technology and assembled to realize a damper. Vision-based technology is used to catch as much possible information on the actual behavior of the SMA elements during the tests.

The report of the test mainly aims at showing the feasibility of such a test procedure. Actually, the information collected includes both the component of the motion at several points along the specimen profile. One could add several bits of information, in terms of quantitative results, by a detailed reading of the output from the tracking process. Furthermore, the re-elaboration of the in-plane displacement components of the single markers along the U-shaped elements could lead the analyst to plot the hysteresis loops on-gone by the SMA alloy at different points.

Future work is expected in finding a camera showing better features in terms of pixel resolution and time recording, but also in terms of required storage memory.

Acknowledgments

The authors are grateful for the financial support from the Research Grants Council of Hong Kong through the GRF Project (No. PolyU 152246/18E). The findings and opinions expressed in this paper are solely those of the authors and do not represent the view of the sponsor.

References

Casciati F., Casciati S., Faravelli L. and Marzi A. (2011), "Fatigue damage accumulation in a Cu-based shape memory alloy", *CMC*., **23**(3), 287-306.

Casciati, F., Faravelli, L. and Petrini, L. (1998), "Energy dissipation in shape memory alloy devices", *Comput. Aided Civil Infrastruct. Eng*., **13**, 433-442. DOI: 10.1111/0885-9507.00121.

Casciati, F., Faravelli, L. and Hamdaoui, K. (2007), "Performance of a base isolator with shape memory alloy bars", *Earthq. Eng. Eng. Vib*., **6**, 401-4088. DOI:10.1007/s11803-007-0787-2.

Casciati, S. and Faravelli, L. (2008), "Structural components in shape memory alloy for localized energy dissipation", *Comp. Struct*., **86**(3-5), 330-339. DOI: 10.1016/j.compstruc.2007.01.037.

Casciati, S., Faravelli, L. and Vece, M. (2017), "Investigation on the fatigue performance of Ni-Ti thin wires", *Struct. Control Health Monit*., **24**(1), Article Number: e1855. DOI: 10.1002/stc.1855.

Casciati, S., Torra, V. and Vece, M. (2018), "Local effects induced by dynamic load self-heating in NiTi wires of shape memory alloys", *Struct. Control Health Monit*., **25**(4), Article Number: e2134. DOI: 10.1002/stc.2134.

Pan, B., Qian, K., Xie, H. and Asundi, A. (2009), "Two-dimension digital image correlation for in-plane displacement and strain measurement: a review", *Meas. Sci. Technol*., **20**, 062001. DOI: 10.1088/0957-0233/20/6/062001.

Pan, B., Yu, L.P. and Zhang, Q.B. (2018), "Review of single-camera stereo-digital image correlation techniques for full-field 3D shape and deformation measurement", *Sci. China-Technol. Sci.*, **61**(1), 2-20. DOI:10.1007/s11431-017-9090-x.

Sony, S., Laventure, S. and Sadhu, A. (2019), "A literature review of next-generation smart sensing technology in structural health monitoring", *Struct. Control Health Monit*., **26**, e2321. DOI: 10.1002/stc.2321.

Wang B. and Zhu S. (2018), "Superelastic SMA U-shaped dampers with self-centering functions", *Smart Mater. Struct*., **27** 055003 (14pp). DOI:10.1088/1361-665X/aab52d.

Wu, L.J., Casciati, F. and Casciati, S. (2014), "Dynamic testing of a laboratory model via vision-based sensing", *Eng. Struct*., **60**, 113-125. DOI: 10.1016/j.engstruct.2013.12.002.

Wu, L.J. and Casciati, F. (2014), "Local positioning systems versus structural monitoring: a review", *Struct. Control Health Monit*., **21**, 1209-1221. DOI:10.1002/stc.1643.

Ye, X.W., Ni, Y.Q., Wai, T.T., Wong, K.Y., Zhang, X.M. and Xu, F. (2013), "A vision-based system for dynamic displacement measurement of long-span bridges: algorithm and verification", *Smart Struct. Syst.*, **12**(3-4), 363-379. https://doi.org/10.12989/sss.2013.12.3_4.363.

Ye, X.W., Dong, C.Z. and Liu, T. (2016a), "Image-based structural dynamic displacement measurement using different multi-object tracking algorithms", *Smart Struct. Syst.*, **17**(6), 935-956. https://doi.org/10.12989/sss.2016.17.6.935.

Ye, X.W., Dong, C.Z. and Liu, T. (2016b), "Force monitoring of steel cables using vision-based sensing technology: methodology and experimental verification", *Smart Struct. Syst.*, **18**(3), 585-599. https://doi.org/10.12989/sss.2016.18.3.585.

Zhao, X. and Zhang, Y. (2019), "Bolt loosening angle detection technology using deep learning", *Struct. Control Health Monit*., **26**(1): e2291. DOI: 10.1002/stc.2292.